Energy Minimization of RIS-Assisted Cooperative UAV-USV MEC Network

Yangzhe Liao, Yuanyan Song, Siyu Xia, Yi Han, Ning Xu and Xiaojun Zhai

***Abstract*—Unmanned surface vehicles (USVs) are becoming increasingly significant in fulfilling integrated sensing, computing and communication with the emergence of bidirectional computation tasks. However, QoS provisioning is still challenging since USVs are restricted with limited on-board resources and direct links between them and shore-based terrestrial base stations (TBSs) are frequently blocked. This paper proposes a novel reconfigurable intelligent surface (RIS)-assisted cooperative unmanned aerial vehicle (UAV)-USV mobile edge computing (MEC) network architecture, where RIS-mounted tethered UAV (TUAV) and rotary-wing UAVs (RUAVs) are collaboratively utilized to serve USVs. RUAVs energy minimization is formulated by jointly considering TUAV hovering altitude, RIS phase shift vector, RUAV service selection indicator and RUAVs turning points. A heuristic solution is proposed to tackle the formulated problem, where the original problem is first decoupled into three subproblems, e.g., the joint optimization of RIS phase shift vector and TUAV hovering altitude subproblem, RUAVs service selection indicators subproblem and RUAVs turning points subproblem, each of which is solved by the proposed modified alternative direction method of multiplier (ADMM) algorithm, the proposed enhanced simulated annealing (ESA) algorithm and the proposed successive convex approximation (SCA)-based algorithm. In this way, the challenging problem can be efficiently solved iteratively. The results show that the proposed solution can decrease RUAVs energy consumption by nearly 29% compared to numerous selected advanced algorithms. Moreover, the performance of the proposed solution regarding typical penalty coefficients and number of RIS reflecting elements is investigated.**

***Index Terms*—Unmanned Surface Vehicles, Unmanned Aerial Vehicle, Mobile Edge Computing, Reconfigurable Intelligent Surface, Energy Minimization.**

I. Introduction

A. Research Background

In recent years, the inland waterway multi-robot system of unmanned surface vehicles (USVs) has attracted significant attention from academia and industry due to its technical excellence in data collection and execution in shallow and restricted water areas [1]. With the speedy progress of the emergence of bidirectional computation tasks, USVs have been widely recognized in fulfilling integrated sensing, computing and communication, which allows them to play an increasingly important role in handling a list of novel services, such as remote control and intelligent navigation [2]. In particular, a bidirectional computation task comprises two parts, one of which is generated by USV sensors and the other of which proactively originates from shore-based terrestrial base stations (TBSs). However, due to the limited communication and computing capabilities, USVs are still struggling to satisfy the ever-increasing quality of service (QoS) requirements of computation-intensive and latency-sensitive tasks. Moreover, the direct links between UAVs and TBSs are frequently obstructed due to the harsh environment; even though USVs are allowed to offload tasks to mobile edge computing (MEC) servers, which are placed next to TBS for execution, it is still challenging to promise QoS of USVs task execution since some offloaded tasks cannot be successfully delivered [3-4].

Empowered by cooperative unmanned aerial vehicle (UAV)-USV MEC platform, UAVs have been widely utilized performing as flying MEC servers to serve USVs communication and computation cooperation in a timely manner [5-6]. In particular, the rapid development of UAVs has brought a revolutionary paradigm shift in wireless data transmission to facilitate highly flexible and on-demand deployment of communication infrastructures. Even though combining UAVs and USVs brings numerous technical advantages, it is still challenging to design UAVs trajectory and resource allocation for cooperative UAV-USV MEC network. The situation may become even more difficult for battery-empowered UAVs to serve USVs bidirectional computation tasks with hard time window constraints since UAVs flight energy consumption is extremely high.

Thanks to the rapid development of reconfigurable intelligent surface (RIS), RIS-assisted wireless communications have been expansively explored as one of the most promising solutions to configure smart radio environments [3,7]. In particular, RIS-assisted wireless data transmission is capable of realizing satisfactory transmission quality and coverage improvement by designing RIS reflection coefficients. Moreover, RISs are generally fabricated with lightweight and conformal geometry, which are suitable for mounting with UAVs. In this respect, UAVs technical weaknesses, such as limited on-board batteries, high flight power consumption and insufficient service duration, can be remarkably enhanced while RISs can enjoy high flexibility rather than just coating on building surfaces. The situation may become more optimistic due to the dynamic deployments of tethered UAVs (TUAVs). Especially each TUAV can receive a stable power supply with a prolonged lifetime and realize a higher payload in comparison with untethered UAVs. As a result, TUAV-mounted RIS may not only be able to enhance wireless link quality between UAVs and USVs, but also can decrease energy consumption via

This work was supported in part by the Natural Science Foundation of China under Grant No. 52201417 and Grant No. 52261160383; in part by National Key R&D Program of China under Grant No. 2021ZD0114600; and in part by Shenzhen Science and Technology Program under Grant No. JCYJ20220818102002005. *(Corresponding authors: Ning Xu; Siyu Xia)*

Y. Liao, Y. Song, S. Xia, Y. Han and N. Xu are Wuhan University of Technology, Wuhan, China, 430070. X. Zhai is with University of Essex, Colchester, UK, CO4 3SQ.

jointly considering UAVs trajectories and RIS phase shift vector when serving resource-limited USVs [8].

B. Related Works

1) Energy Minimization of RIS-Assisted UAV MEC Networks: Thanks to the rapid developments of metasurfaces, RIS has been widely recognized as one potential solution to create a controllable wireless environment by smartly adjusting signal electromagnetic properties, including incident signal phase shift and reflection angle, to realize various purposes with near-zero energy consumption. In this way, RIS-mounted UAVs are expected to boost MEC network performance by offering satisfactory line-of-sight (LOS) links between UAVs and ground mobile devices. The authors of [9] installed RIS on the building surface to assist data offloading from mobile devices to UAVs. Mei *et al.* investigated the network energy-efficiency maximization of RIS-assisted UAV MEC network and derived the possibility function to describe direct link quality between each UAV and each mobile device [10]. Aiming to minimize UAV energy consumption, the authors of [11] formulated a network energy efficiency maximization problem by jointly considering UAV trajectory, RIS passive beamforming and MEC resource allocation. The results verified that the available transmission distance between MEC server and ground mobile devices could be considerably prolonged via RIS-mounted UAVs. The authors of [4] proposed a RIS-assisted hybrid UAV-terrestrial network architecture to serve USVs tasks execution with soft time window and formulated USVs energy minimization problem by jointly considering USVs offloading decisions, computing capability, TBS beamforming vector and RIS phase shift-vector design. Note that with the emergence of USVs bidirectional computation tasks, UAVs energy consumption optimization of RIS-assisted UAV MEC network may become highly challenging since USVs locally generated and remote input data should be cooperatively considered; however, very few works have explored how to jointly determine UAV hovering altitude and RIS phase shift vector.

2) Look Forward of Bidirectional Data Computation in RIS-Assisted Wireless Inland Waterway Communication Networks: The authors of [12] proposed a novel bidirectional computation task model and formulated a network energy minimization problem. The results showed that the network energy consumption could be considerably decreased by dynamically allocating network computing resources. The authors of [13] proposed a novel LOS/non-line-of-sight (NLOS) hybrid wireless communication model for RIS-assisted UAV MEC network and pointed out that USVs energy efficiency could be remarkably enhanced by jointly optimizing UAV flying and hovering altitude. The authors of [14] proposed a novel RIS-assisted hybrid UAV-terrestrial network architecture to serve USVs bidirectional tasks with soft time window. The results revealed that USVs energy consumption could be considerably decreased by optimizing bandwidth allocation. However, one should be aware that most existing works cannot be directly applied to decrease USVs bidirectional computation task energy consumption for the following reasons. First, inland waterways environments are generally more complicated in comparison with terrestrial wireless communications; wireless data transmission may simultaneously suffer LOS and NLOS, which results in severe signal attenuation. Moreover, the large amount of the existing solutions cannot be directly employed in handling USVs bidirectional computation tasks with hard time window since they only considered one-way computation or bidirectional computation tasks with soft time window; it is extremely challenging to jointly schedule UAVs service selection indicator, UAVs trajectories and RIS phase shift vector when serving a number of USVs.

C. The Main Contributions

According to the above-mentioned research background, unlike most of the research that assumes each USV computation task can only be implemented via either local execution mode or UAV execution mode, two types of UAVs are jointly considered to serve USVs bidirectional computation tasks, where one RIS-mounted tethered UAV (TUAV) is utilized to assist USVs remote data transmission with a dynamic hovering altitude and a set of rotary-wing UAVs (RUAVs) are integrated with MEC servers to offer computing services with the low altitude. In this way, wireless data transmission quality can be significantly enhanced and the majority of USVs bidirectional tasks energy consumption can be transferred from resource-hungry USVs to RUAVs. The main contributions of this paper are summarized as follows.

- This paper proposes a novel RIS-assisted cooperative UAV-USV MEC network architecture, where RIS-mounted TUAV and flying MEC servers RUAVs are cooperatively deployed to serve USVs computation and communication cooperation. In particular, RIS-mounted TUAV can dynamically decide its flying altitude and obtain a substantial power source since it is connected to TBS via cable. Moreover, each RUAV can dynamically determine its service selection indicator and trajectory to serve USVs according to the wireless link quality and USVs task size.
- RUAVs flight energy consumption minimization problem is formulated by jointly considering TUAV hovering altitude, RIS phase shift vector, RUAV service selection indicator and RUAVs turning points. To tackle the formulated challenging problem, a heuristic solution is proposed. First, we decouple the original problem into three subproblems, e.g., the joint optimization of RIS phase shift vector and TUAV hovering altitude subproblem, RUAVs service selection indicators subproblem and RUAVs turning points subproblem. Moreover, a modified alternative direction method of multiplier (ADMM) algorithm, an enhanced simulated annealing (ESA) algorithm and successive convex approximation (SCA)-based algorithm are proposed to efficiently solve each subproblem, respectively. In this way, the formulated challenging problem can be efficiently solved in an iteratively manner.

The rest of this paper is summarized as follows. The proposed RIS-assisted cooperative UAV-USV MEC network architecture and the formulated RUAVs flight energy consumption minimization problem are demonstrated in Section II. The proposed solution is presented in Section III. The selected

key performance metrics of the proposed solution along with several benchmarks are revealed in Section IV. Section V concludes the paper.

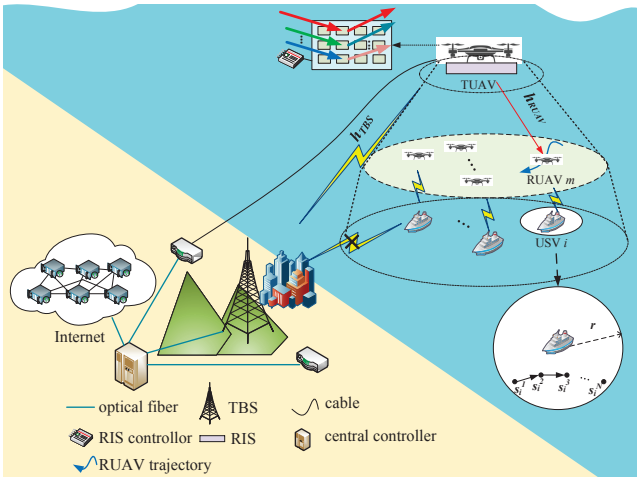

Fig. 1: The proposed network architecture.

II. System Model and Problem Formulation

The proposed wireless inland waterway RIS-assisted cooperative UAV-USV MEC network architecture to support USVs data collection, transmission and computation is demonstrated in Fig. 1. In this system, TBS is equipped with L-antennas and one K RIS reflecting elements TUAV is dynamically dispatched and forms virtual clusters with TBS. The set of $\mathcal{M}$ single-antenna RUAVs is deployed to collect data generated by USVs via the predetermined trajectory. Moreover, each RUAV $m \in \mathcal{M}$ is integrated with a MEC server. During each equal-length time slot, each USV $i \in \mathcal{I}$ requests a bidirectional computation task U_i to be executed, which can be characterized by a five-tuple $U_i \triangleq \{D_i^l, D_i^o, F_i, [X_i, Y_i]\}$, where D_i^l and D_i^o represent the input data size (in bits) generated by USV i itself and originate proactively from the Internet, respectively. F_i denotes the required number of CPU cycles to execute U_i. $[X_i, Y_i]$ indicates the earliest and latest service time to execute U_i. In particular, D_i^l and D_i^o are only able to start to execute not earlier than X_i and need to finish execution not later than Y_i. Moreover, the direct link between TBS and each RUAV is assumed to be severely blocked.

The system is established based on three-dimensional Cartesian coordinates, where coordinates of TBS and each USV i can be denoted by $\boldsymbol{q_{TBS}} \in \mathbb{R}^3$ and $\boldsymbol{q_i} \in \mathbb{R}^3$, respectively. The coordinate of TUAV is denoted by $\boldsymbol{q_{TUAV}} \in \mathbb{R}^3$, where horizontal coordinate is fixed and flying altitude is time-varying. RUAVs are assumed to fly at a fixed altitude, which is lower than TUAV flying altitude. Following [15], each TUAV-mounted RIS transmission link is assumed based on long-term statistical CSI to reduce the signaling and hardware implementation complexity. In addition, we assume that MEC server and central controller is aware of task data size, time window constraints, coordinate of each USV and CSI as a *prior*.

A. USVs Data Collection Model

The trajectory of each RUAV m to serve USV i can be divided into a list of N segments, denoted by $\boldsymbol{q_i} \triangleq \{\boldsymbol{q_i^{m_1}}, \boldsymbol{q_i^{m_2}}, \ldots, \boldsymbol{q_i^{m_N}}\}$[1], $i \in \mathcal{I}, m \in \mathcal{M}, n \in \mathcal{N}$, where $\boldsymbol{q_i^{m_n}}$ represents n-th turning point of RUAV m. Following [16], the trajectory of each RUAV m between any two successive turning points is assumed to be a straight line.

Let δt_i^n be the arrival time when RUAV m arriving turning point $\boldsymbol{q_i^{m_n}}$. The trajectory of RUAV m between any two successive turning points can be expressed as

$$\Delta \boldsymbol{q_i^m} = \boldsymbol{q_i^{m_{n-1}}} + \frac{v(t-\delta t_i^{n-1})}{||\boldsymbol{q_i^{m_n}} - \boldsymbol{q_i^{m_{n-1}}}||}(\boldsymbol{q_i^{m_n}} - \boldsymbol{q_i^{m_{n-1}}}), \quad t \in [\delta t_i^{n-1}, \delta t_i^n], i \in \mathcal{I}, m \in \mathcal{M}, n \in \mathcal{N}, \tag{1}$$

where v is the flight speed of each RUAV m, which can be assumed as constant.

Let the transmission power and the maximum transmission distance of each USV i be p_i^{tr} and R, respectively. One has

$$\mathcal{C}1 : ||\boldsymbol{q_i^{m_n}} - \boldsymbol{q_i}|| \leq R, i \in \mathcal{I}, m \in \mathcal{M}, n \in \mathcal{N}. \tag{2}$$

The achievable data transmission rate between each USV i and RUAV m can be expressed as

$$C_i^m(\Delta \boldsymbol{q_i^m}) = B_i^{ul} \log_2(1 + \frac{p_i^{tr} h_0}{||\boldsymbol{q_i} - \Delta \boldsymbol{q_i^m}||^2 \sigma^2}), i \in \mathcal{I}, \tag{3}$$

where B_i^{ul} and σ^2 represent the allocated uplink bandwidth and noise variance, respectively. h_0 indicates the channel power gain at the reference distance $d_0 = 1\ m$.

The throughput of RUAV m to serve USV i can be expressed as

$$C_i^m = \sum_{n=1}^{N} \int_0^1 B_i^{ul} \log_2(1 + \frac{p_i^{tr} h_0}{||\boldsymbol{q_i} - \Delta \boldsymbol{q_i^m}(z_i^m)||^2 \sigma^2} dz_i^m, \tag{4}$$

where z_i^m represents the normalization of $\Delta \boldsymbol{q_i^m}$.

To promise data transmission quality, the throughput of each USV i cannot be less than D_i^l. One has

$$\mathcal{C}2 : C_i^m \geq D_i^l, i \in \mathcal{I}. \tag{5}$$

B. RIS-Assisted Data Transmission and Task Execution Model

After each USV i completes data collection, the corresponding RUAV needs to keep hovering status at $\boldsymbol{q_i^{m_N}}$ to receive downlink data D_i^o via TUAV-mounted RIS. The corresponding RIS phase shift vector to serve USV i can be denoted by $\boldsymbol{\theta_i} = [\theta_i^1, \theta_i^2, \ldots, \theta_i^K]^T$, where each element of $\boldsymbol{\theta_i}$ should satisfy

$$\mathcal{C}3 : \theta_i^k \in [0, 2\pi], k \in \{1, 2, \ldots, K\}, i \in \mathcal{I}. \tag{6}$$

In the same manner with [6], we assume that each RIS element follows the full reflection. In this manner, the reflection coefficient matrix of RIS can be expressed as $\boldsymbol{\Theta_i} = \text{diag}(\theta_i^1, \theta_i^2, \ldots, \theta_i^K)$. Moreover, we assume that the communication link between TBS and each TUAV-mounted RIS simultaneously suffers LOS and NLOS conditions [17]. The

[1]RUAVs recharging platform can be regarded as a special USV without generating any task and its coordinate $\boldsymbol{q_0}$ is assumed known a *priori*.

probability of LOS regarding each TBS-RIS link can be represented by a function of elevation angle θ_{TBS}, which can be expressed as

$$P_{LOS}(\theta_{TBS}) = \frac{1}{1 + A_{TBS}e^{-B_{TBS}(\theta_{TBS} - A_{TBS})}}, \tag{7}$$

where A_{TBS} and B_{TBS} are both transmission environmental-related parameters.

Let H_i be TUAV hovering altitude. One has

$$\mathcal{C}4 : H_{min} \leq H_i \leq H_{max}, i \in \mathcal{I}, \tag{8}$$

where H_{min} and H_{max} represent the minimum and the maximum TUAV hovering altitude, respectively.

The corresponding path loss (PL) exponent β_{TBS} can be given as

$$\beta_{TBS}(\theta_{TBS}) = P_{LOS}(\theta_{TBS})u_{TBS} + v_{TBS}, \tag{9}$$

where u_{TBS} and v_{TBS} are constants, which depend on wireless transmission environment.

The baseband channel of TBS $\rightarrow$ TUAV-mounted RIS can be considered as Rician fading channel [18]. The corresponding $\boldsymbol{h}_{TBS} \in \mathbb{R}^{L \times K}$ can be expressed as

$$\boldsymbol{h}_{TBS} = \sqrt{\rho_0 d_{TBS}^{-\beta_{TBS}}}\left(\sqrt{\frac{R_{TBS}}{R_{TBS}+1}}\boldsymbol{g}_{TBS}^{LOS} + \sqrt{\frac{1}{R_{TBS}+1}}\boldsymbol{g}_{TBS}^{NLOS}\right), \tag{10}$$

where $d_{TBS} = ||\boldsymbol{q}_{TUAV} - \boldsymbol{q}_{TBS}||$ is the distance between TBS and each TUAV-mounted RIS. ρ_0 denotes the channel power at the reference distance $d_0 = 1\ m$. R_{TBS} represents the Rician coefficient and $\boldsymbol{g}_{TBS}^{NLOS}$ is the small scale fading. $\boldsymbol{g}_{TBS}^{LOS}$ can be given as[2]

$$\boldsymbol{g}_{TBS}^{LOS} = \begin{bmatrix} 1 & e^{-j\frac{2\pi d}{\lambda}\phi_{1,r}} & \cdots & e^{-j\frac{2(K-1)\pi d}{\lambda}\phi_{1,r}} \\ \vdots & \vdots & \ddots & \vdots \\ 1 & e^{-j\frac{2\pi d}{\lambda}\phi_{l,r}} & \cdots & e^{-j\frac{2(K-1)\pi d}{\lambda}\phi_{l,r}} \\ \vdots & \vdots & \ddots & \vdots \\ 1 & e^{-j\frac{2\pi d}{\lambda}\phi_{L,r}} & \cdots & e^{-j\frac{2(K-1)\pi d}{\lambda}\phi_{L,r}} \end{bmatrix}, \tag{11}$$

where each $\phi_{l,r}$ indicates the cosine of the incident angle from l-th antenna of TBS to TUAV-mounted RIS.

TUAV-mounted RIS $\rightarrow$ RUAV link is assumed as LOS. Let baseband channel of TUAV-mounted RIS $\rightarrow$ RUAV m be $\boldsymbol{h}_{RUAV} \in \mathbb{R}^{K \times 1}$, which can be expressed as

$$\boldsymbol{h}_{RUAV} = \sqrt{\rho_0 d_{RUAV}^{-\beta_{RUAV}}}\boldsymbol{g}_{RUAV}^{LOS}, \tag{12}$$

where $d_{RUAV} = ||\boldsymbol{q}_{\boldsymbol{i}}^{\boldsymbol{m_N}} - \boldsymbol{q}_{TUAV}||$ is the distance between RUAV and TUAV-mounted RIS. β_{RUAV} denotes PL exponent of $\boldsymbol{h}_{RUAV}$, which is a constant. $\boldsymbol{g}_{RUAV}^{LOS} = [1, e^{-j\frac{2\pi d}{\lambda}\phi_{m,r}}, \cdots, e^{-j\frac{2(K-1)\pi d}{\lambda}\phi_{m,r}}]$ and $\phi_{m,r}$ indicates the cosine of the incident angle from RUAV m to each TUAV-mounted RIS.

The corresponding downlink SNR of RUAV can be expressed as

$$\gamma_i^{dl} = \frac{p_{TBS}^{tr}||\boldsymbol{w}_{\boldsymbol{i}}^{\boldsymbol{H}}(\boldsymbol{h}_{TBS}\boldsymbol{\Theta}_{\boldsymbol{i}}\boldsymbol{h}_{RUAV})||^2}{\sigma^2}, i \in \mathcal{I}, \tag{13}$$

[2]According to Snell's law, the incident angle can be reasonably assumed equal to the reflected angle when each RIS element follows the full reflection.

where p_{TBS}^{tr} is the transmission power of TBS and s_i is the transmitted data symbol with average unity power, i.e., $\mathbb{E}(|s_i|^2) = 1$. $\boldsymbol{w_i} \in \mathbb{R}^{L \times 1}$ indicates the downlink beamforming vector designed by TBS to serve each USV i. $\boldsymbol{w_i^H}$ is the Hermitian matrix of $\boldsymbol{w_i}$.

The instantaneous RIS-assisted downlink channel capacity can be given as

$$C_i^{dl} = B_m^{dl}\log_2(1 + \gamma_i^{dl}), i \in \mathcal{I}, \tag{14}$$

where B_m^{dl} is the allocated downlink bandwidth for RUAV m. The corresponding transmission time cost of D_i^o can be expressed as

$$t_i^{dl} = \frac{D_i^o}{C_i^{dl}}, i \in \mathcal{I}. \tag{15}$$

Note that each RUAV m can only be able to start executing U_i after receiving D_i^o. The time cost of RUAV m to execute U_i can be given as

$$t_i^{exe} = \frac{F_i}{f_m}, i \in \mathcal{I}, \tag{16}$$

where f_m denotes the computing capability of RUAV m.

C. USVs Data Collection, Transmission and Computation Model

Consider any three successive USVs served by RUAV m, e.g., USV i^-, i and i^+. One should note that RUAV m can only be able to depart from $\boldsymbol{q}_{\boldsymbol{i}}^{\boldsymbol{m_N}}$ to $\boldsymbol{q}_{\boldsymbol{i^+}}^{\boldsymbol{m_1}}$ to collect $D_{i^+}^l$ of USV i^+ after finishing execute U_i. Let ζ_{i,i^+}^m be service selection indicator for RUAV m, where $\zeta_{i,i^+}^m = 1$ represents RUAV m selects to serve USV i^+ after finishing serving USV i and otherwise $\zeta_{i,i^+}^m = 0$. One has

$$\mathcal{C}5 : \zeta_{i,i^+}^m \in \{0,1\}, i, i^+ \in \mathcal{I}, m \in \mathcal{M}. \tag{17}$$

Since each RUAV m needs to take off from RUAVs recharging platform at the beginning of each service slot, one has

$$\mathcal{C}6 : \sum_{i \in \mathcal{I}} \zeta_{0,i}^m = 1, m \in \mathcal{M}. \tag{18}$$

Since each RUAV m needs to return to RUAVs recharging platform to get recharged, one has

$$\mathcal{C}7 : \sum_{i \in \mathcal{I}} \zeta_{i,0}^m = 1, m \in \mathcal{M}. \tag{19}$$

Note that each RUAV m cannot start to serve data collection for USV i earlier than X_i. δt_i^1 of each RUAV m to arrive $\boldsymbol{q}_{\boldsymbol{i}}^{\boldsymbol{m_1}}$ should not be earlier than X_i. One has

$$\mathcal{C}8 : \delta t_i^1 \geq X_i, i \in \mathcal{I}, \tag{20}$$

where $\delta t_i^1 \triangleq \sum_{i^- \in \mathcal{I}} \zeta_{i^-,i}^m (\delta t_{i^-}^N + t_{i^-}^{dl} + t_{i^-}^{exe} + \frac{||\boldsymbol{q}_{\boldsymbol{i}}^{\boldsymbol{m_1}} - \boldsymbol{q}_{\boldsymbol{i^-}}^{\boldsymbol{m_N}}||}{v})$.

After finishing data collection, RUAV m should keep hovering status at $\boldsymbol{q}_{\boldsymbol{i}}^{\boldsymbol{m_N}}$ to download D_i^o from TBS via TUAV-mounted RIS. Each U_i should finish execution not late than Y_i, one has

$$\mathcal{C}9 : \delta t_i^1 + \frac{\sum_{n=1}^{N-1} ||\boldsymbol{q}_{\boldsymbol{i}}^{\boldsymbol{m_{n+1}}} - \boldsymbol{q}_{\boldsymbol{i}}^{\boldsymbol{m_n}}||}{v} + t_i^{dl} + t_i^{exe} \leq Y_i, i \in \mathcal{I}. \tag{21}$$

The flight energy consumption of RUAV m to serve USV i can be expressed as

$$E_i^m = \sum_{i^-,i\in\mathcal{I}} p_{RUAV}\frac{\zeta_{i^-,i}^m||\boldsymbol{q_i^{m_1}}-\boldsymbol{q_{i^-}^{m_N}}||+\sum_{n=1}^{N-1}||\boldsymbol{q_i^{m_{n+1}}}-\boldsymbol{q_i^{m_n}}||}{v}, \tag{22}$$

where p_{RUAV} represents flight power of each RUAV.

D. Problem Formulation

In this paper, we aim to minimize RUAVs flight energy consumption by jointly considering TUAV hovering altitude $\boldsymbol{H}\triangleq\{H_i, i\in\mathcal{I}\}$, RIS phase shift vector $\boldsymbol{\theta}\triangleq\{\theta_i^k, i\in\mathcal{I}, k\in\mathcal{K}\}$, RUAVs service selection indicator $\boldsymbol{\zeta}\triangleq\{\zeta_{i,i^+}^m, i, i^+\in\mathcal{I}, m\in\mathcal{M}\}$ and RUAVs turning points $\boldsymbol{q}\triangleq\{\boldsymbol{q_i^{m_n}}, i\in\mathcal{I}, m\in\mathcal{M}, n\in\mathcal{N}\}$, which can be formulated as

$$\begin{aligned}\mathcal{P}1: \min_{\boldsymbol{H},\boldsymbol{\theta},\boldsymbol{\zeta},\boldsymbol{q}} \ & \sum_{m\in\mathcal{M}}\sum_{i\in\mathcal{I}} E_i^m \\ s.t. \quad & \mathcal{C}1-\mathcal{C}9.\end{aligned} \tag{23}$$

III. The Proposed Solution

In this section, a heuristic solution is proposed to solve the formulated challenging problem $\mathcal{P}1$. We first decouple the original problem $\mathcal{P}1$ into three subproblems, e.g., the joint optimization of RIS phase shift vector and TUAV hovering altitude subproblem $\mathcal{P}1.1$, RUAVs service selection indicators subproblem $\mathcal{P}1.2$ and RUAVs turning points subproblem $\mathcal{P}1.3$. To tackle $\mathcal{P}1.1$, we first transform $\mathcal{P}1.1$ into a list of I parallel sub-problems, where each of which can be efficiently solved via the proposed ADMM-based algorithm and thus one can obtain the optimized TUAV hovering altitude. Moreover, $\mathcal{P}1.2$ can be solved using the proposed ESA algorithm and thus RUAV service selection indicator $\boldsymbol{\zeta}$ can be obtained. Subsequently, we decouple $\mathcal{P}1.3$ into M parallel sub-problems according to the updated M RUAV service set as obtained in solving $\mathcal{P}1.2$; each subproblem can be solved via utilizing the proposed SCA-based algorithm and thus one can obtain optimized RUAV turning points. In this way, one can obtain the feasible solution to the challenging problem $\mathcal{P}1$. The detailed information regarding the proposed solution is given as follows.

A. The Joint Optimization of TUAV Hovering Altitude $\boldsymbol{H}$ and RIS Phase Shift Vector $\boldsymbol{\theta}$

Given any feasible $\boldsymbol{\zeta}$ and $\boldsymbol{q}$, one can observe that $\mathcal{P}1$ can be divided into a list of sub-problems, which can be efficiently solved in parallel. After remove irrelevant parameters according to Eqs. (13)-(15), $\mathcal{P}1$ can be reduced as

$$\begin{aligned}\mathcal{P}1.1: \max_{H_i,\boldsymbol{\theta_i}} \ & ||\boldsymbol{w_i^H}(\boldsymbol{h}_{TBS}\boldsymbol{\Theta_i}\boldsymbol{h}_{RUAV})||^2 \\ s.t. \quad & \mathcal{C}3-\mathcal{C}4.\end{aligned} \tag{24}$$

Given any feasible H_i, $\mathcal{P}1.1$ can be further reduced as

$$\begin{aligned}\mathcal{P}1.1.1: \max_{\boldsymbol{\theta_i}} \ & ||\boldsymbol{w_i^H}(\boldsymbol{h}_{TBS}\boldsymbol{\Theta_i}\boldsymbol{h}_{RUAV})||^2 \\ s.t. \quad & \mathcal{C}3.\end{aligned} \tag{25}$$

As such, one can obtain the optimal solution to $\mathcal{P}1.1.1$ as $\boldsymbol{\theta_i^*}=\{\theta_i^{1*},\cdots,\theta_i^{K*}\}$, where $\theta_i^{k*}=-\arg(\boldsymbol{\Omega_i}(k))$ and $\boldsymbol{\Omega_i}=\boldsymbol{h}_{TBS}\mathrm{diag}(\boldsymbol{h}_{RUAV})$ [19].

After obtain the optimal $\boldsymbol{\theta^*}$, $\mathcal{P}1.1$ can be further reduced as

$$\begin{aligned}\mathcal{P}1.1.2: \max_{H_i} \ & d_{TBS}^{-\beta_{TBS}} d_{RUAV}^{-\beta_{RUAV}} \\ s.t. \quad & \mathcal{C}4.\end{aligned} \tag{26}$$

Define $f_1(H_i) = v_{TBS}\log(\sqrt{d_{b,r}^2+H_i^2}) + \beta_{USV}\log(\sqrt{d_{r,m}^2+H_i^2})$ and $f_2(H_i)=\frac{u_{TBS}\log(\sqrt{d_{b,r}^2+H_i^2})}{1+A_{TBS}e^{-B_{TBS}(\theta_{TBS}-A_{TBS})}}$, where $d_{b,r}$ and $d_{r,m}$ denote horizontal projection distance between TBS and TUAV-mounted RIS, TUAV-mounted RIS and RUAV m, respectively. One can transform the objective function of $\mathcal{P}1.1.2$ into the following

$$\begin{aligned}&\log(d_{TBS}^{-\beta_{TBS}} d_{RUAV}^{-\beta_{RUAV}}) \\ &= -\beta_{TBS}\log d_{TBS} - \beta_{RUAV}\log d_{RUAV} \\ &= -v_{TBS}\log(\sqrt{d_{b,r}^2+H_i^2}) - \beta_{RUAV}\log(\sqrt{d_{r,m}^2+H_i^2}) \\ &\quad - \frac{u_{TBS}\log(\sqrt{d_{b,r}^2+H_i^2})}{1+A_{TBS}e^{-B_{TBS}(\theta_{TBS}-A_{TBS})}} \\ &= -f_1(H_i) - f_2(H_i).\end{aligned} \tag{27}$$

In this way, $\mathcal{P}1.1.2$ can be reformulated as

$$\begin{aligned}\tilde{\mathcal{P}}1.1.2: \min_{H_i} \ & f_1(H_i)+f_2(H_i) \\ s.t. \quad & \mathcal{C}4.\end{aligned} \tag{28}$$

Note that $\tilde{\mathcal{P}}1.1.2$ is still challenging to tackle for the following reasons. First, $f_1(H_i)$ is non-convex with respect to H_i. Moreover, H_i is closely coupled with the denominator of $f_2(H_i)$. Inspired by [20], ADMM is utilized to decouple $\tilde{\mathcal{P}}1.1.2$. After introduce the duplicated variable $\hat{H}_i, i\in\mathcal{I}$ to substitute H_i in $f_2(H_i)$, one has

$$\mathcal{C}10: H_i=\hat{H}_i, i\in\mathcal{I}. \tag{29}$$

In this way, $\tilde{\mathcal{P}}1.1.2$ can be reformulated as

$$\begin{aligned}\overline{\mathcal{P}}1.1.2: \min_{H_i} \ & f_1(H_i)+f_2(\hat{H}_i), \\ s.t. \quad & \mathcal{C}4, \mathcal{C}10.\end{aligned} \tag{30}$$

Note that $\overline{\mathcal{P}}1.1.2$ is separable along with H_i and $\hat{H}_i$. As such, one can alternatively update H_i and $\hat{H}_i$ to obtain the feasible solution to $\overline{\mathcal{P}}1.1.2$. The detailed information is summarized as follows.

The update of H_i: In each r-th iteration, the optimization problem of H_i can be formulated as

$$\begin{aligned}\overline{\mathcal{P}}1.1.2.1: \min_{H_i} \ & f_1(H_i)+\frac{\rho}{2}(H_i-\hat{H}_i^{\,r-1})^2 \\ s.t. \quad & \mathcal{C}4,\end{aligned} \tag{31}$$

where ρ is the penalty parameter. Note that $\mathcal{P}1.2.2.1$ is still challenging to tackle since $f_1(H_i)$ is non-convex with respect to H_i, which makes $\mathcal{P}1.1.2.1$ cannot be directly solved by using the existing high-efficient algorithms.

One can observe that $v_{TBS}\log(\sqrt{d_{b,r}^2+H_i^2})$ and $\beta_{USV}\log(\sqrt{d_{r,m}^2+H_i^2})$ are concave with respect to H_i^2.

The upper bound of $v_{TBS}\log(\sqrt{d_{b,r}^2+H_i^2})$ can be determined by employing the first-order Taylor expansion [21], which can be expressed as

$$\begin{aligned} &v_{TBS}\log(\sqrt{d_{b,r}^2+H_i^2}) \\ &\triangleq \frac{v_{TBS}}{2}\log(d_{b,r}^2+(H_i^{r-1})^2)+\frac{v_{TBS}(H_i^2-(H_i^{r-1})^2)}{2(d_{b,r}^2+(H_i^{r-1})^2)}. \end{aligned} \tag{32}$$

Note that $\beta_{USV}\log(\sqrt{d_{r,m}^2+H_i^2})$ is identical to $v_{TBS}\log(\sqrt{d_{b,r}^2+H_i^2})$. After remove irrelavant parameters, the upper bound of $f_1(H_i)$ in each r-th iteration can be given as

$$f_1^{ub}(H_i)\triangleq\frac{v_{TBS}(H_i^2-(H_i^{r-1})^2)}{2(d_{b,r}^2+(H_i^{r-1})^2)}+\frac{\beta_{RUAV}(H_i^2-(H_i^{r-1})^2)}{2(d_{r,m}^2+(H_i^{r-1})^2)}. \tag{33}$$

As such, $\overline{\mathcal{P}}1.1.2.1$ can be reformulated as

$$\begin{aligned} &\hat{\mathcal{P}}1.1.2.1: \min_{H_i} f_1^{ub}+\frac{\rho}{2}(H_i-\hat{H}_i^{r-1})^2 \\ &s.t. \qquad\qquad \mathcal{C}4. \end{aligned} \tag{34}$$

One can observe that $\hat{\mathcal{P}}1.2.2.1$ is a convex optimization problem, which can be solved by CVX [22].

The update of $\hat{H}_i$: The optimization problem of $\hat{H}_i$ in each r-th iteration can be formulated as

$$\begin{aligned} &\mathcal{P}1.1.2.2: \min_{\hat{H}_i} f_2(\hat{H}_i) \\ &s.t. \qquad \mathcal{C}4, \mathcal{C}10. \end{aligned} \tag{35}$$

Note that $\hat{H}_i$ can be expressed as follows

$$\hat{H}_i = d_{b,r}\tan\theta_{TBS}. \tag{36}$$

As such, $f_2(\hat{H}_i)$ can be rewritten as

$$f_2(d_{b,r}\tan\theta_{TBS})=\frac{u_{TBS}\log(\sqrt{d_{b,r}^2+d_{b,r}^2\tan^2\theta_{TBS}})}{1+A_{TBS}e^{-B_{TBS}(\theta_{TBS}-A_{TBS})}}. \tag{37}$$

According to Dinkelbach's approach [23], $\mathcal{P}1.1.2.2$ can be reformulated as

$$\begin{aligned} &\hat{\mathcal{P}}1.1.2.2: \min_{\theta_{TBS}} -f_2(\theta_{TBS}^{r-1})(1+A_{TBS}e^{-B_{TBS}(\theta_{TBS}-A_{TBS})}) \\ &\quad +u_{TBS}\log(\sqrt{d_{b,r}^2+d_{b,r}^2\tan^2\theta_{TBS}})+\frac{\rho}{2}w(\theta_{TBS}-\hat{\theta}_{TBS}^{r-1})^2 \\ &s.t. \qquad \hat{\mathcal{C}}4: \theta_{TBS}^{min}\le\theta_{TBS}\le\theta_{TBS}^{max}, \end{aligned} \tag{38}$$

where $\hat{\theta}_{TBS}=\arctan(\frac{H_i^r}{d_{b,r}})$ and w is the scale coefficient. θ_{TBS}^{min} and θ_{TBS}^{max} represent the minimum and maximum values of θ_{TBS}, respectively.

Note that u_{TBS} is a negative constant and thus $f_2(d_{b,r}\tan\theta_{TBS})$ is negative with respect to any feasible θ_{TBS}. According to **Proposition 1**, the approximation of $u_{TBS}\log(\sqrt{d_{b,r}^2+d_{b,r}^2\tan^2\theta_{TBS}})$ can be given as $u_{TBS}\log(\sqrt{d_{b,r}^2+d_{b,r}^2\tan^2\theta_{TBS}^{r-1}})+\frac{u_{TBS}\tan\theta_{TBS}^{r-1}\sec^2\theta_{TBS}^{r-1}}{1+\tan^2\theta_{TBS}^{r-1}}(\theta_{TBS}-\theta_{TBS}^{r-1})$.

Proposition 1: The approximation of $u_{TBS}\log(\sqrt{d_{b,r}^2+d_{b,r}^2\tan^2\theta_{TBS}})$ can be given as $u_{TBS}\log(\sqrt{d_{b,r}^2+d_{b,r}^2\tan^2\theta_{TBS}^{r-1}})+\frac{u_{TBS}\tan\theta_{TBS}^{r-1}\sec^2\theta_{TBS}^{r-1}}{1+\tan^2\theta_{TBS}^{r-1}}(\theta_{TBS}-\theta_{TBS}^{r-1})$.

Proof. Note that $u_{TBS}\log(\sqrt{d_{b,r}^2+d_{b,r}^2\tan^2\theta_{TBS}})=\frac{u_{TBS}}{2}\log(d_{b,r}^2+d_{b,r}^2\tan^2\theta_{TBS})$. The first-order derivative of $\frac{u_{TBS}}{2}\log(d_{b,r}^2+d_{b,r}^2\tan^2\theta_{TBS})$ is $\frac{2\tan\theta_{TBS}\sec^2\theta_{TBS}}{1+\tan^2\theta_{TBS}}$. The second-order derivative of $u_{TBS}\log(\sqrt{d_{b,r}^2+d_{b,r}^2\tan^2\theta_{TBS}})$ is shown in Eq. (39).

Note that $2+2\tan^2\theta_{TBS}-\sec^2\theta_{TBS}=\frac{2\cos^2\theta_{TBS}+2\sin^2\theta_{TBS}-1}{\cos^2\theta_{TBS}}=\frac{1}{\cos^2\theta_{TBS}}\ge 0$. In this way, one has $(\frac{u_{TBS}}{2}\log(d_{b,t}^2+d_{b,t}^2\tan^2\theta_{TBS}))''\le 0$.

As such, $u_{TBS}\log(\sqrt{d_{b,r}^2+d_{b,r}^2\tan^2\theta_{TBS}})$ is cancave with respect to θ_{TBS}. As such, the upper bound of $u_{TBS}\log(\sqrt{d_{b,r}^2+d_{b,r}^2\tan^2\theta_{TBS}})$ can be given as $u_{TBS}\log(\sqrt{d_{b,r}^2+d_{b,r}^2\tan^2\theta_{TBS}^{r-1}})+\frac{u_{TBS}\tan\theta_{TBS}^{r-1}\sec^2\theta_{TBS}^{r-1}}{1+\tan^2\theta_{TBS}^{r-1}}(\theta_{TBS}-\theta_{TBS}^{r-1})$. The proof is completed. □

$\hat{\mathcal{P}}1.1.2.2$ can be reformulated as

$$\begin{aligned} &\overline{\mathcal{P}}1.2.2.2: \min_{\theta_{TBS}} -f_2(\theta_{TBS}^{r-1})(1+A_{TBS}e^{-B_{TBS}(\theta_{TBS}-A_{TBS})}) \\ &+\frac{u_{TBS}\tan\theta_{TBS}^{r-1}\sec^2\theta_{TBS}^{r-1}}{1+\tan^2\theta_{TBS}^{r-1}}(\theta_{TBS}-\theta_{TBS}^{r-1})+\frac{\rho}{2}w(\theta_{TBS}-\hat{\theta}_{TBS}^{r-1})^2 \\ &s.t. \qquad\qquad \hat{\mathcal{C}}4. \end{aligned} \tag{40}$$

One can see that $\overline{\mathcal{P}}1.1.2.2$ is a convex optimization problem, which can be solved by CVX. In this manner, the optimized TUAV hovering altitude H_i^* can be obtained. Let ϵ_{ADMM} and r_{ADMM}^{max} be the error control parameter and the maximum number of iterations of the proposed ADMM-based algorithm. The proposed algorithm can be regarded as convergence when $|H_i-\hat{H}_i|\le\epsilon_{ADMM}$ or $r_{ADMM}=r_{ADMM}^{max}$ The detailed information of the proposed ADMM-based algorithm can be found in **Algorithm 1**.

Algorithm 1: The proposed ADMM-based algorithm

```
divide P1.1 into a list of sub-problems
consider each sub-problem
for i ∈ I do
    initialize H_i^1 = H_min, Ĥ_i^1 = H_max, r_ADMM = 1
    while |H_i − Ĥ_i| ≤ ε_ADMM or r_ADMM ≤ r_ADMM^max do
        solve P̂1.1.2.1 and obtain H_i^{r_ADMM}
        solve P̄1.1.2.2 and obtain θ_TBS
        update scale coefficient w
        r_ADMM = r_ADMM + 1
    end
end
```

$$
\begin{aligned}
&(\frac{u_{TBS}}{2}\log(d_{b,r}^2+d_{b,r}^2\tan^2\theta_{TBS}))''=(\frac{u_{TBS}}{2}\frac{2\tan\theta_{TBS}\sec^2\theta_{TBS}}{1+\tan^2\theta_{TBS}})'\\
&=\frac{u_{TBS}}{2}\frac{(2\sec^4\theta_{TBS}+4\sec^2\theta_{TBS}\tan^2\theta_{TBS})(1+\tan^2\theta_{TBS})-4\tan^2\theta_{TBS}\sec^4\theta_{TBS}}{(1+\tan^2\theta_{TBS})^2}\\
&=\frac{u_{TBS}}{2}\frac{2\sec^4\theta_{TBS}-2\sec^4\theta_{TBS}\tan^2\theta_{TBS}+4\sec^2\theta_{TBS}\tan^2\theta_{TBS}+4\sec^2\theta_{TBS}\tan^4\theta_{TBS}}{(1+\tan^2\theta_{TBS})^2}\\
&=\frac{u_{TBS}}{2}\frac{2\sec^4\theta_{TBS}+2\sec^2\theta_{TBS}\tan^2\theta_{TBS}(2+2\tan^2\theta_{TBS}-\sec^2\theta_{TBS})}{(1+\tan^2\theta_{TBS})^2},
\end{aligned}
\tag{39}
$$

B. The Optimization of RUAVs Service Selection Indicator

Given any feasible $\boldsymbol{\theta}$, $\boldsymbol{H}$ and $\boldsymbol{q}$, $\mathcal{P}1$ can be reduced as

$$
\begin{aligned}
&\mathcal{P}1.2: \min_{\boldsymbol{\zeta}} \quad \sum_{m\in\mathcal{M}}\sum_{i\in\mathcal{I}} p_u \frac{\zeta_{i^-,i}^m ||\boldsymbol{q_i^{m_1}}-\boldsymbol{q_{i^-}^{m_N}}||}{v}\\
&s.t. \qquad\qquad \mathcal{C}5-\mathcal{C}9.
\end{aligned}
\tag{41}
$$

One can observe that $\mathcal{P}1.2$ can be regarded as a multiple traveling salesman problem with time window, which has been proven as NP-hard and highly challenging to tackle [24]. Inspired by [25], an enhanced simulated annealing algorithm (ESA) is proposed to tackle $\mathcal{P}1.2$. The key steps of the proposed ESA algorithm are given as follows.

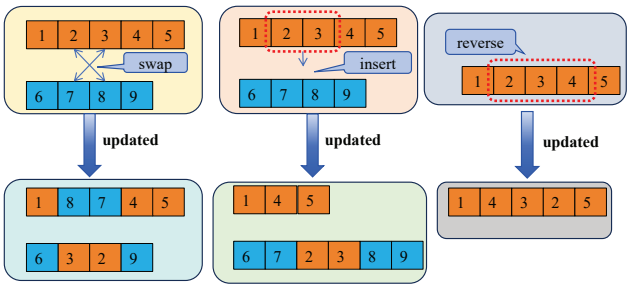

Fig. 2: The example of the proposed three perturb operations.

Perturb Operation: Let $\mathcal{R}_r$ be the obtained feasible solution to $\mathcal{P}1.2$ in r-th iteration. To enhance the diversity in the search region, three different perturb operators are utilized to obtain new solution $\mathcal{R}^{new}$. The example regarding swap operation, insert operation and reverse operation is shown in Fig. 2. The roulette wheel method is utilized to generate $\mathcal{R}^{new}$, where the weighting factor of each operation can be assumed as equal.

Swap operation: Randomly select two RUAV service sets and then randomly select one element in each service set and swap the selected two elements.

Insert operation: Randomly select two RUAV service sets and then randomly select y consecutive elements from one of the selected service sets, where y should be less than the number of elements in the selected service set. Then, insert into two successive elements in another service set.

Reverse operation: Randomly select one service set and then choose y consecutive elements, where y should be less than the number of elements in the selected service set. Then, reverse the order of the selected elements.

Fitness evaluation: All obtained solution should satisfy constraint $\mathcal{C}8$ and $\mathcal{C}9$, a penalty based method is proposed, the fitness value of $\mathcal{R}^{new}$ can be obtained via the following fitness function

$$
\begin{aligned}
&f(\mathcal{R}^{new})\\
&=\sum_{m\in\mathcal{M}}\sum_{i\in\mathcal{I}} p_{RUAV}\frac{\zeta_{i^-,i}^m ||\boldsymbol{q_i^{m_1}}-\boldsymbol{q_{i^-}^{m_N}}||}{v}+\mu\sum_{i\in\mathcal{I}}X_i-\delta t_i^1\\
&+\nu\sum_{i\in\mathcal{I}}\delta t_i^1+\frac{\sum_{n=1}^{N-1}||\boldsymbol{q_i^{m_{n+1}}}-\boldsymbol{q_i^{m_n}}||}{v}+t_i^{dl}+t_i^{exe}-Y_i,
\end{aligned}
\tag{42}
$$

where μ and ν are the penalty coefficients.

Acceptance criterion: Note that unlike the widely used nature-inspired optimization algorithms, such as genetic algorithm and differential evolution (DE) algorithm, simulated annealing algorithm can accept $\mathcal{R}^{new}$ as $\mathcal{R}^{r+1}$ even if $f(\mathcal{R}^{new}) \le f(\mathcal{R}^r)$. The acceptance criterion can be given as follows

$$
\mathcal{R}^{r+1}=\begin{cases}\mathcal{R}^{new}, & f(\mathcal{R}^{new})\ge f(\mathcal{R}^r),\\ & \text{or } rand\le e^{-(f(\mathcal{R}^r)-f(\mathcal{R}^{new}))/T^r},\\ \mathcal{R}^r, & \text{otherwise},\end{cases}
\tag{43}
$$

where $e^{-(f(\mathcal{R}^r)-f(\mathcal{R}^{new}))/T^r}$ is the probability to accept $\mathcal{R}^{new}$ as $\mathcal{R}^{r+1}$ when $f(\mathcal{R}^{new}) \le f(\mathcal{R}^r)$. T^r represents the temperature parameter of simulated annealing in r-th iteration. To promise the convergence of the proposed ESA, the acceptance probability should keep decreasing as the number of iterations increases. To this respect, one can update T^r via $T^{r+1}=\alpha T^r$, where α is a constant ranging from 0 to 1. The proposed ESA algorithm can be regarding reaching convergence when $r_{ESA}=r_{ESA}^{max}$, where r_{ESA}^{max} represents the maximum number of iterations. In this manner, the optimized USV service indicator $\boldsymbol{\zeta}^*$ can be obtained. The detailed information of the proposed ESA algorithm is given in **Algorithm 2**.

C. The Optimization of RUAVs Turning Points

Given any feasible $\boldsymbol{\theta}$, $\boldsymbol{H}$ and RUAV service set $\mathcal{R}_m, m\in\mathcal{M}$, $\mathcal{P}1$ can be reduced as

$$
\begin{aligned}
&\mathcal{P}1.3: \min_{\boldsymbol{q}} \quad \sum_{m\in\mathcal{M}}\sum_{i\in\mathcal{R}_m\bigcup\{0\}} E_i^m,\\
&s.t. \qquad \mathcal{C}1-\mathcal{C}2, \mathcal{C}8-\mathcal{C}9.
\end{aligned}
\tag{44}
$$

One can observe that $\mathcal{P}1.3$ can be divided into M subproblems according to M RUAV service set, where each subproblem can be solved in parallel.

Algorithm 2: The proposed ESA algorithm

initialize $\mathcal{R}^1$, $r_{ESA}=1$
while $r_{ESA} \le r_{ESA}^{max}$ **do**
  $\mathcal{R}^{r_{ESA}+1}=\mathcal{R}^{r_{ESA}}$
  utilize roulette wheel method to select one perturb operator from the proposed three perturb operators
  perform the selected perturb operator to $\mathcal{R}^{r_{ESA}}$ to generate $\mathcal{R}^{new}$
  if $f(\mathcal{R}^{new}) \ge f(\mathcal{R}^{r_{ESA}})$ or $rand \le e^{-(f(\mathcal{R}^{r_{ESA}})-f(\mathcal{R}^{new}))/T^{r_{ESA}}}$ **then**
    update $\mathcal{R}^{r_{ESA}+1}=\mathcal{R}^{new}$
  end
  update $T^{r_{ESA}+1}=\alpha T^{r_{ESA}}$
  update $r_{ESA}=r_{ESA}+1$
end

Consider each sub-problem, $\mathcal{P}1.3$ can be further reduced as

$$\mathcal{P}1.3.1: \min_{\boldsymbol{q_i}} \sum_{i\in\mathcal{R}_m\bigcup\{0\}} p_{RUAV}\frac{\zeta_{i^-,i}^m||\boldsymbol{q_i^{m_1}}-\boldsymbol{q_{i^-}^{m_N}}||+\sum_{n=1}^{N-1}||\boldsymbol{q_i^{m_{n+1}}}-\boldsymbol{q_i^{m_n}}||}{v} \quad (45)$$
$$s.t. \qquad \mathcal{C}1-\mathcal{C}2, \mathcal{C}8-\mathcal{C}9.$$

One can see that $\mathcal{P}1.3.1$ is a non-convex optimization problem due to the non-convexity of $\mathcal{C}2$, $\mathcal{C}8$ and $\mathcal{C}9$. Inspired by [16], we aim to relax $\mathcal{P}1.3$ into a convex optimization problem via considering convex approximation for $\mathcal{C}2$, $\mathcal{C}8$ and $\mathcal{C}9$.

Note that each RUAV trajectory can be regarded as a curve with a list of turning points. The throughput of each USV i, denoted by C_i^n, can be rewritten as follows

$$\begin{aligned} C_i^m &= \sum_{n=1}^{N}\int_0^1 B_i^{ul}\log_2(1+\frac{p_i^{tr}h_0}{||\boldsymbol{q_i}-\boldsymbol{\Delta q_i^{m_n}}(z)||^2\sigma^2})dz. \\ &= \lim_{N\to\infty}\sum_{n=1}^{N} B_i^{ul}\log_2(1+\frac{p_i^{tr}h_0}{||\boldsymbol{q_i}-\boldsymbol{q_i^{j_n}}||^2\sigma^2})\frac{||\boldsymbol{q_i^{j_n}}-\boldsymbol{q_i^{j_{n-1}}}||}{v}. \end{aligned} \quad (46)$$

In this paper, we assume that N is large enough to realize the satisfactory transmission rate between any two successive turning points e.g., $\boldsymbol{q_i^{m_{n-1}}}$ and $\boldsymbol{q_i^{m_n}}$ by $C_i^m(\boldsymbol{q_i^{m_n}})$ [26]. In this way, C_i^m can be relaxed as

$$\hat{C}_i^m = \sum_{n=1}^{N} B_i^{ul}\log_2(1+\frac{p_i^{tr}h_0}{||\boldsymbol{q_i}-\boldsymbol{q_i^{m_n}}||^2\sigma^2})\frac{||\boldsymbol{q_i^{m_n}}-\boldsymbol{q_i^{m_{n-1}}}||}{v}. \quad (47)$$

Consequently, $\mathcal{C}2$ can be rewritten as

$$\hat{\mathcal{C}}2: \hat{C}_i^m \ge D_i^l. \quad (48)$$

One should be aware that traditional SCA cannot be directly utilized to approximate $\hat{C}_i^m$ since $B_i^{ul}\log_2(1+\frac{p_i^{tr}h_0}{||\boldsymbol{q_i}-\boldsymbol{q_i^{m_n}}||^2\sigma^2})$ and $\frac{||\boldsymbol{q_i^{m_n}}-\boldsymbol{q_i^{m_{n-1}}}||}{v}$ are closely coupled. To tackle this challenging problem, ADMM is utilized to decouple $\hat{\mathcal{C}}2$.

After introduce a duplicated variable $\hat{\boldsymbol{q}}_{\boldsymbol{i}} \triangleq \{\hat{\boldsymbol{q}}_{\boldsymbol{i}}^{\boldsymbol{m_n}}, n\in\mathcal{N}\}$ of $\boldsymbol{q_i}$, one has

$$\mathcal{C}11: \hat{\boldsymbol{q}}_{\boldsymbol{i}} = \boldsymbol{q_i}, i\in\mathcal{I}. \quad (49)$$

In this way, $\hat{C}_i^m$ can be rewritten as

$$\overline{C}_i^m = \sum_{n=1}^{N} B_i^{ul}\log_2(1+\frac{p_i^{tr}h_0}{||\boldsymbol{q_i}-\boldsymbol{q_i^{m_n}}||^2\sigma^2})\frac{||\hat{\boldsymbol{q}}_{\boldsymbol{i}}^{\boldsymbol{m_n}}-\hat{\boldsymbol{q}}_{\boldsymbol{i}}^{\boldsymbol{m_{n-1}}}||}{v}. \quad (50)$$

One can observe that $\overline{C}_i^m$ is separable along $\boldsymbol{q_i}$ and $\hat{\boldsymbol{q}}_{\boldsymbol{i}}$. As such, the solution to $\mathcal{P}1.3.1$ can be obtained via respectively update $\boldsymbol{q_i}$ and $\hat{\boldsymbol{q}}_{\boldsymbol{i}}$ in an iterative manner. Consider concave approximation of $\overline{C}_i^m$, one can see that $\log_2(1+\frac{p_i^{tr}h_0}{||\boldsymbol{q_i}-\boldsymbol{q_i^{m_n}}||^2})$ is convex with respect to $||\boldsymbol{q_i}-\boldsymbol{q_i^{m_n}}||^2$. In this way, the lower bound of $\log_2(1+\frac{p_i^{tr}h_0}{||\boldsymbol{q_i}-\boldsymbol{q_i^{m_n}}||^2})$ can be given as

$$\begin{aligned} &\log_2(1+\frac{p_i^{tr}h_0}{||\boldsymbol{q_i}-\boldsymbol{q_i^{m_n}}||^2}) \\ &\triangleq Z_i^r - \dot{Z}_i^r(||\boldsymbol{q_i}-\boldsymbol{q_i^{m_n}}||^2 - ||\boldsymbol{q_i}-\boldsymbol{q_i^{m_n,r}}||^2), \end{aligned} \quad (51)$$

where $Z_i^r = \log_2(1+\frac{p_i^{tr}h_0}{||\boldsymbol{q_i}-\boldsymbol{q_i^{m_n,r-1}}||^2})$ and $\dot{Z}_i^r = \frac{p_i^{tr}h_0}{||\boldsymbol{q_i}-\boldsymbol{q_i^{m_n,r-1}}||^2+p_i^{tr}h_0||\boldsymbol{q_i}-\boldsymbol{q_i^{m_n,r-1}}||}$. $\boldsymbol{q_i^{m_n,r-1}}$ represents the optimized turning point n of RUAV m when serving USV i in each $r-1$ iteration.

The lower bound of $||\hat{\boldsymbol{q}}_{\boldsymbol{i}}^{\boldsymbol{m_n}}-\hat{\boldsymbol{q}}_{\boldsymbol{i}}^{\boldsymbol{m_{n-1}}}||$ can be obtained via using the first-order Taylor expansion, one has

$$\begin{aligned} &||\hat{\boldsymbol{q}}_{\boldsymbol{i}}^{\boldsymbol{m_n}}-\hat{\boldsymbol{q}}_{\boldsymbol{i}}^{\boldsymbol{m_{n-1}}}|| \\ &\triangleq ||\hat{\boldsymbol{q}}_{\boldsymbol{i}}^{\boldsymbol{m_n,r-1}}-\hat{\boldsymbol{q}}_{\boldsymbol{i}}^{\boldsymbol{m_{n-1},r-1}}|| \\ &+2(\hat{\boldsymbol{q}}_{\boldsymbol{i}}^{\boldsymbol{m_n}}-\hat{\boldsymbol{q}}_{\boldsymbol{i}}^{\boldsymbol{m_{n-1}}})(\hat{\boldsymbol{q}}_{\boldsymbol{i}}^{\boldsymbol{m_n,r-1}}-\hat{\boldsymbol{q}}_{\boldsymbol{i}}^{\boldsymbol{m_{n-1},r-1}})^T \end{aligned} \quad (52)$$

The lower bound of $\overline{C}_i^m$ can be given as

$$\begin{aligned} \overline{C}_i^{m,lb} &\triangleq \sum_{n=1}^{N} B_i^{ul}(Z_i^r - \dot{Z}_i^r(||\boldsymbol{q_i}-\boldsymbol{q_i^{m_n}}||^2 - ||\boldsymbol{q_i}-\boldsymbol{q_i^{m_n,r}}||^2)) \\ &\cdot(||\hat{\boldsymbol{q}}_{\boldsymbol{i}}^{\boldsymbol{m_n,r-1}}-\hat{\boldsymbol{q}}_{\boldsymbol{i}}^{\boldsymbol{m_{n-1},r-1}}|| \\ &+2(\hat{\boldsymbol{q}}_{\boldsymbol{i}}^{\boldsymbol{m_n}}-\hat{\boldsymbol{q}}_{\boldsymbol{i}}^{\boldsymbol{m_{n-1}}})(\hat{\boldsymbol{q}}_{\boldsymbol{i}}^{\boldsymbol{m_n,r-1}}-\hat{\boldsymbol{q}}_{\boldsymbol{i}}^{\boldsymbol{m_{n-1},r-1}})^T). \end{aligned} \quad (53)$$

To this respect, one can utilize convex approximation to transform $\hat{\mathcal{C}}2$ into

$$\overline{\mathcal{C}}2: \overline{C}_i^{m,lb} \ge D_i^l. \quad (54)$$

The analysis of $\mathcal{C}8$: Define the auxiliary variable $\kappa_i = X_i - \delta t_{i-}^N - t_{i-}^{dl} - t_{i-}^{exe}, i, i^-\in\mathcal{I}$. In this way, $\mathcal{C}8$ can be rewritten as

$$\bar{\mathcal{C}}8: ||\boldsymbol{q_i^{m_1}}-\boldsymbol{q_{i-}^{m_N}}|| \ge v\kappa_i. \quad (55)$$

One can utilize SCA to approximate $||\boldsymbol{q_i^{m_1}}-\boldsymbol{q_{i-}^{m_N}}||$. In this way, $\bar{\mathcal{C}}8$ can be transformed into

$$\begin{aligned} \hat{\mathcal{C}}8: &2(\boldsymbol{q_i^{m_1}}-\boldsymbol{q_{i-}^{m_N}})(\boldsymbol{q_i^{m_1,r-1}}-\boldsymbol{q_{i-}^{m_N}})^T \\ &\ge v\kappa_i - ||\boldsymbol{q_i^{m_1,r-1}}-\boldsymbol{q_{i-}^{m_N}}||. \end{aligned} \quad (56)$$

The analysis of $\mathcal{C}9$: Define the auxiliary variable $r_i^{dl}, i\in\mathcal{I}$, $\mathcal{C}9$ can be transformed into a convex constraint as follows

$$\hat{\mathcal{C}}9: \delta t_i^1 + \frac{\sum_{n=1}^{N-1}||\boldsymbol{q_i^{m_{n+1}}}-\boldsymbol{q_i^{m_n}}||}{v} + \frac{D_i^o}{r_i^{dl}} + t_i^{exe} \le Y_i, \quad i\in\mathcal{I}. \quad (57)$$

To promise the equality between $\hat{\mathcal{C}}9$ and $\mathcal{C}9$, one has

$$\mathcal{C}12: C_i^{dl} \geq r_i^{dl}, i \in \mathcal{I}. \tag{58}$$

Note that $\mathcal{C}12$ is non-convex constraint. After substitute the feasible RIS phase shift vector, C_i^{dl} can be rewritten as follows according to Eqs. (13)-(14). One has

$$C_i^{dl} = B_m^{dl}\log_2(1+\frac{p_{TBS}^{tr}||\boldsymbol{w_i^H}||^2}{\sigma^2||\boldsymbol{q}_{TBS}-\boldsymbol{q}_{TUAV}||^{\beta_{TBS}}||\boldsymbol{q}_{TUAV}-\boldsymbol{q_i^{m_N}}||^{\beta_{RUAV}}}). \tag{59}$$

Note that C_i^{dl} is convex with respect to $||\boldsymbol{q}_{TUAV}-\boldsymbol{q_i^{m_N}}||^{\beta_{RUAV}}$. One can utilize first-order Taylor expansion to obtain the lower bound of C_i^{dl}, which can be expressed as Eq. (60).

In this way, $\mathcal{P}1.3.1$ can be transformed into

$$\begin{aligned}\hat{\mathcal{P}}1.3.1: \min_{\boldsymbol{q_i}} & \sum_{i\in\mathcal{R}_m\bigcup\{0\}} p_{RUAV}\frac{\zeta_{i^-,i}^m||\boldsymbol{q_i^{m_1}}-\boldsymbol{q_{i^-}^{m_N}}||}{v} \\ & + p_{RUAV}\frac{\sum_{n=1}^{N-1}||\boldsymbol{q_i^{m_{n+1}}}-\boldsymbol{q_i^{m_n}}||}{v} + \frac{\xi}{2}||\boldsymbol{q_i}-\hat{\boldsymbol{q}}_{\boldsymbol{i}}||_F^2 \\ s.t. \quad & \mathcal{C}1, \overline{\mathcal{C}}2, \hat{\mathcal{C}}8, \hat{\mathcal{C}}9, \hat{\mathcal{C}}12.\end{aligned} \tag{61}$$

where ξ is the penalty coefficient of $\mathcal{C}11$. One can observe that $\hat{\mathcal{P}}1.3.1$ is a convex optimization problem with respect to $\boldsymbol{q_i}$ and $\hat{\boldsymbol{q}}_{\boldsymbol{i}}$, which can be efficiently solved by CVX. As such, the optimized each UAV i trajectory $\boldsymbol{q}_i^*$ can be obtained. The proposed SCA-based algorithm can be regarded as reach convergence when $r_{SCA} = r_{SCA}^{max}$ or $||\boldsymbol{q_i}-\hat{\boldsymbol{q}}_{\boldsymbol{i}}||_F \leq \epsilon_{SCA}$, where r_{SCA}^{max} is the maximum number of iterations and ϵ_{SCA} is the error control parameter. The detailed information of the proposed SCA-based algorithm can be found in **Algorithm 3**.

Algorithm 3: The proposed ADMM-SCA-based algorithm

```
divide P1.3 into M parallel subproblems
consider each sub-problem
initialize q_i^1, q̂_i^1, r_SCA = 1
while r_SCA ≤ r_SCA^max or ||q_i − q̂_i||_F ≤ ε_SCA do
    transform C2 into C̄2
    transform C8 into Ĉ8
    introduce Ĉ11
    fix q̂_i = q̂_i^{r_SCA}
    solve P̂1.3.1 and obtain q_i^{r_SCA+1}
    fix q_i = q_i^{r_SCA+1}
    solve P̂1.3.1 and obtain q̂_i^{r_SCA+1}
    update r_SCA = r_SCA + 1
end
```

The framework regarding the proposed solution is summarized in **Algorithm 4**, where r^{max} represents the maximum number of iterations. One should note that in the proposed network, TBS is placed in conjunction with sufficient computing resources, where TBS can efficiently implement the proposed solution and then the obtained optimized parameters can be wirelessly transmitted to TUAV, RUAVs and RIS controller promptly. Moreover, the communication overhead can be assumed ignored since they are considerably smaller than the computation task data size as proved in [27].

Proposition 2: The complexity of **Algorithm 4** can be roughly determined as $\mathcal{O}(r^*(I^{2.5}\log(\frac{1}{\epsilon_{ADMM}}) + r_{ESA}^* + I^{3.5}\log(\frac{1}{\epsilon_{SCA}})))$.

Proof. Let r^* be the minimum required number of iterations for the proposed solution to realize convergence. The complexity of the proposed ADMM algorithm to solve $\mathcal{P}1.1$ is $\mathcal{O}(I^{2.5}\log(\frac{1}{\epsilon_{ADMM}}))$. The complexity of the proposed ESA algorithm to solve $\mathcal{P}1.2$ is $\mathcal{O}(r_{ESA}^*)$, where r_{ESA}^* represents the number of iterations for the proposed ESA algorithm to reach convergence. The complexity of the proposed SCA algorithm to solve $\mathcal{P}1.3$ is $\mathcal{O}(I^{3.5}\log(\frac{1}{\epsilon_{SCA}}))$. As such, the complexity of **Algorithm 4** can be roughly expressed as $\mathcal{O}(r^*(I^{2.5}\log(\frac{1}{\epsilon_{ADMM}}) + r_{ESA}^* + I^{3.5}\log(\frac{1}{\epsilon_{SCA}})))$. □

Algorithm 4: The framework of the proposed solution

```
initialize q^1, r = 1
while r ≤ r^max do
    given q^r, solve P1.1 via Algorithm 1 and obtain H^{r+1}
    given H^{r+1}, q^r, solve P1.2 via Algorithm 2 and obtain R^{r+1}
    given H^{r+1}, R^r, solve P1.3 via Algorithm 3 and obtain q^{r+1}
    update r = r + 1
end
```

IV. Performance Evaluation

This section evaluates and compares the selected key performance metrics of the proposed solution with numerous benchmark algorithms. All experiments are conducted in MATLAB with CVX toolbox on a PC with Intel Core i7-12700K CPU @3.70GHz and 16GB RAM. The significant simulation parameters are given as follows. USVs are randomly distributed in a square area of 350 m × 350 m. The input data size generated by each USV and originating from the Internet ranges from $[1, 10] \times 10^6$ bits and $[1, 10] \times 10^8$, respectively. The required CPU cycles to execute each task are set as $[1, 10] \times 10^6$ and the computation capability of each RUAV is 5×10^6 CPU cycles/s. The earliest and latest service times range from $[1, 500]$ s and $[200, 600]$ s, respectively. The flight altitude of RUAV is set as 25 m. The maximum TUAV and minimum hovering altitudes are 200 m and 50 m. We assume that wireless communication channels are perfectly estimated, RUAV-USV communication link is assumed as LOS and set PL coefficients $\beta_{RUAV} = 2$. TBS-RIS communication link suffers LOS and NLOS conditions simultaneously, where the significant parameters of the probability of LOS are set as $A_{TBS} = \frac{\pi}{9}$ and $B_{TBS} = 2$, respectively according to real world measurments [28]. Moreover, the corresponding PL exponent parameters are set as $v_{TBS} = 4$ and $u_{TBS} = -2$. A list of selected advanced algorithms, e.g., Fly-in Fly-out (FIFO)

$$C_i^{dl,lb} \triangleq B_m^{dl}\log_2(1+\frac{p_{TBS}^{tr}||\boldsymbol{w_i^H}||^2}{\sigma^2||\boldsymbol{q}_{TBS}-\boldsymbol{q}_{TUAV}||^{\beta_{TBS}}||\boldsymbol{q}_{TUAV}-\boldsymbol{q}_i^{\boldsymbol{m_N},\boldsymbol{r-1}}||^{\beta_{RUAV}}}) - \frac{p_{TBS}^{tr}||\boldsymbol{w_i^H}||^2(||\boldsymbol{q}_{TUAV}-\boldsymbol{q}_i^{\boldsymbol{m_N}}||^{\beta_{RUAV}}-||\boldsymbol{q}_{TUAV}-\boldsymbol{q}_i^{\boldsymbol{m_N},\boldsymbol{r-1}}||^{\beta_{RUAV}})}{\sigma^2||\boldsymbol{q}_{TBS}-\boldsymbol{q}_{TUAV}||^{\beta_{TBS}}||\boldsymbol{q}_{UAV}-\boldsymbol{q}_i^{\boldsymbol{m_N},\boldsymbol{r-1}}||^{2\beta_{RUAV}}+p_{TBS}^{tr}||\boldsymbol{q_m}-\boldsymbol{q}_i^{\boldsymbol{m_N},\boldsymbol{r-1}}||^{\beta_{RUAV}}}. \quad (60)$$

algorithm, fixed TUAV hovering altitude (FHA) algorithm, gradient descent (GD) algorithm and DE algorithm, are selected and compared with the proposed solution. The details regarding the selected algorithms are given as follows.

FIFO algorithm: As proposed in [29], the trajectory of each RUAV m to serve USV i is assumed as a straight line, which can be determined by a fly-in point and a fly-out point. RUAV m starts to receive D_i^l when arriving at the fly-in point and ends at fly-out points. RUAV m hovers at a fly-out point to receive D_i^o from TBS and then executes U_i by itself. The optimization of TUAV hovering altitude and RUAV service selection indicator is identical to the proposed solution.

FHA algorithm: TUAV is assumed as hovering at the fixed altitude, e.g., $H = 100$ m. The optimization of RUAV trajectory and RUAV service selection indicator is identical to the proposed solution.

GD algorithm: GD algorithm is utilized to optimize TUAV hovering altitude as analyzed in [30]. The optimization of RUAV trajectory and RUAV service selection indicator is identical to the proposed solution.

DE algorithm: DE algorithm is utilized to optimize RUAVs turning points as proposed in [31]. The optimization of TUAV hovering altitude and RUAVs service selection indicator is identical to the proposed solution.

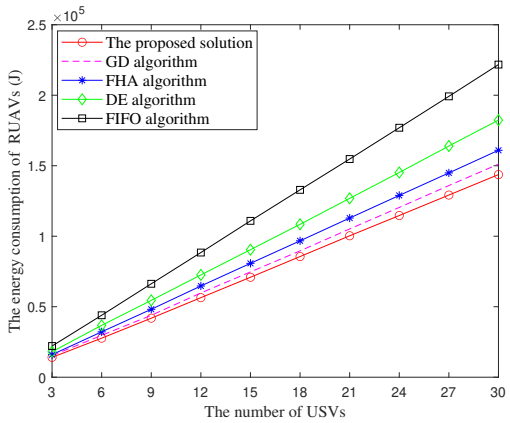

Fig. 3: The energy consumption versus the number of USVs.

Fig. 3 demonstrates RUAVs energy consumption versus the different number of USVs. One can observe that the proposed solution realizes the lowest RUAVs energy consumption in comparison with other algorithms under the same number of USVs. In particular, the proposed solution achieves around 7.0×10^4 J and 1.4×10^5 J when $I = 15$ and 30, respectively. Followed by FHA algorithm with the corresponding values approximately 7.5×10^4 J and 1.5×10^5 J, respectively. FIFO algorithm reaches the worst performance with corresponding

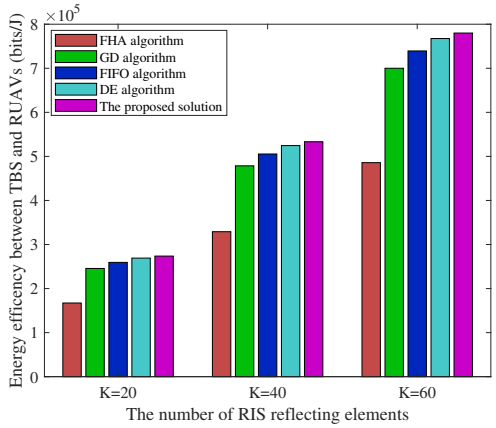

Fig. 4: The energy efficiency between TBS and USVs versus the number of RIS reflecting elements.

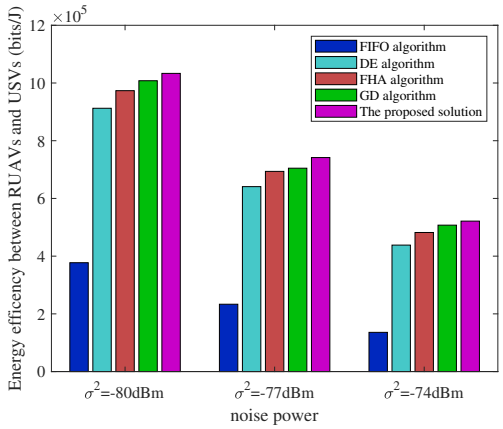

Fig. 5: The energy consumption versus the number of USVs.

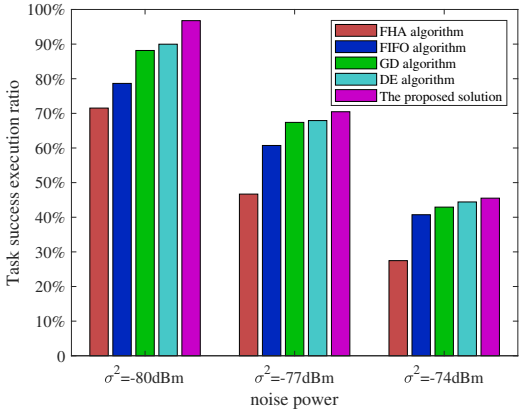

Fig. 6: Task success execution ratio versus noise power.

value at nearly 1.1×10^5 J and 2.1×10^5 J, respectively. This is because the proposed solution is capable of optimizing each RUAV trajectory and thus the corresponding flight distance to receive D_i^o can be considerably decreased. Moreover, the proposed solution can dynamically adjust TUAV hovering altitude according to the channel quality between TBS and RUAVs. As such, the transmission time cost of each RUAV to receive D_i^o can be decreased.

The energy efficiency between TBS and USVs is defined as the energy consumption per bit for TBS to transmit data to USVs. Fig. 4 shows the energy efficiency between TBS and USVs versus the number of RIS reflecting elements. One can observe that energy efficiency between TBS and USV of all algorithms increases with the number RIS reflecting elements increases. Specifically, the proposed solution realizes the best energy efficiency at around 2.8×10^5 bits/J, 5.6×10^5 bits/J and 8.2×10^5 bits/J when $K=20$, $K=40$ and $K=60$, respectively. Followed by DE algorithm with corresponding values of 2.7×10^5 bits/J, 5.3×10^5 bits/J and 7.7×10^5 bits/J. FHA realizes the worst energy efficiency with approximately 1.7×10^5 bits/J, 3.3×10^5 bits/J and 4.8×10^5 bits/J when $K=20$, $K=40$ and $K=60$, respectively. This is because the higher number of RIS reflecting elements can enhance communication link quality. This may involve the fact that with a fixed TUAV hovering altitude, TBS-RUAV communication link may be severely blocked or suffer additional PL caused by inappropriate TUAV hovering altitude.

The energy efficiency between RUAVs and USVs is defined as the energy consumption per bit for USVs to transmit data to RUAVs. Fig. 5 shows energy efficiency between RUAVs and USVs versus different typical noise power. In particular, the proposed solution realizes approximately 1.0×10^6 bits/J, 7.4×10^5 bits/J and 5.2×10^5 bits/J when σ^2=-80 dBm, σ^2=-77 dBm and σ^2=-74 dBm, respectively. Followed by FHA algorithm with corresponding value of 1.0×10^6 bits/J, 7.0×10^5 bits/J and 5.1×10^5 bits/J, respectively. FIFO algorithm realizes the worst energy efficiency with 3.8×10^5 bits/J, 2.3×10^5 bits/J and 1.4×10^5 bits/J when σ^2=-80 dBm, -77 dBm and -74 dBm, respectively. One can observe that energy efficiency decreases with the noise power increasing. This is because higher noise power promises lower SNR to maintain data transmission quality; the distance between each RUAV and USVs is shortened, increasing the time cost for each RUAV to receive D_i^l.

In this paper, task that cannot be successfully executed within its time window can be regarded as failed. In this manner, task success execution ratio can be defined as the percentage of successfully executed tasks. Fig. 6 demonstrates task success execution ratio versus different noise power. One can observe that task success execution ratio of all algorithms keeps decreasing as noise power increases. The proposed solution outperforms other algorithms under the same noise power. In particular, task success execution ratio of the proposed solution is about 97%, 70% and 46% when $\sigma^2=$ -80 dBm, -77 dBm and -74 dBm, respectively, followed by DE algorithm and GD algorithm with corresponding values of 90%, 68%, 44% and 88%, 67%, 43%. FHA algorithm realizes the worst performance with the task success execution ratio at 71%, 46% and 27% when $\sigma^2=$ -80 dBm, -77 dBm and -74 dBm, respectively. One should note that higher noise power may lead to lower SNR and thus the transmission time cost may significantly increase. In addition, the proposed solution can dynamically adjust TUAV hovering altitude according to RUAVs trajectories and communication link status. As such, the downlink data transmission time cost can be considerably reduced.

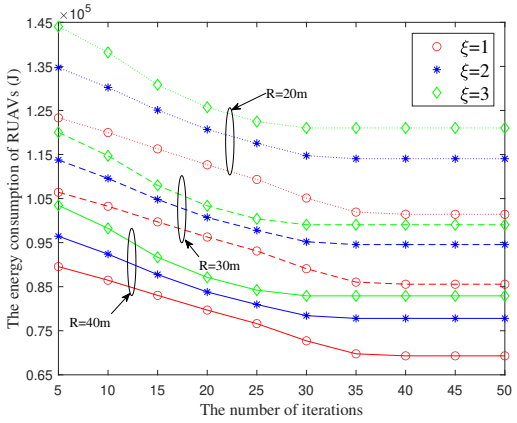

Fig. 7: The energy consumption of RUAVs versus the number of iterations.

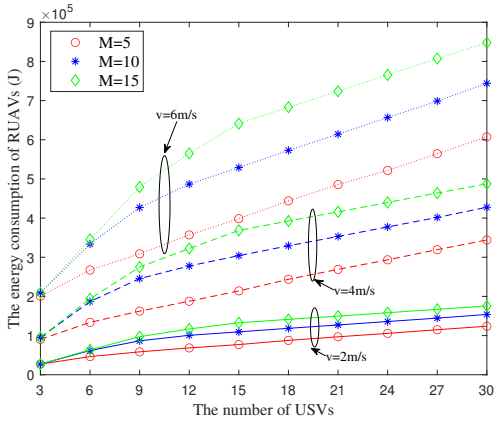

Fig. 8: The energy consumption of RUAVs versus the number of USVs under different typical number of RUAVs.

The typical number of USVs, e.g., $I=15$ is selected for further investigation. Fig. 7 shows the energy consumption of RUAVs versus the number of iterations under different typical ADMM penalty coefficients. One can observe that the higher value of ADMM penalty coefficient promises a lower USVs energy consumption under the same maximum transmission distance R. In particular, when $R=40$ m, RUAVs energy consumption of the proposed solution is around 6.9×10^4 J when $\xi=1$ while this value increases to around 7.8×10^4 J and 8.2×10^4 J when $\xi=2$ and 3, respectively. This is due to the fact that the smaller ADMM penalty coefficients require a higher number of iterations to reach convergence. As such, the proposed solution is capable of reaching a lower energy consumption with a higher number of iterations when

ADMM penalty coefficient is properly determined. Moreover, one can observe that RUAVs energy consumption increases as R decreases. This is because RUAV is capable of flying closer to each USV for data collection when R is appropriately determined.

The typical number of RUAVs, e.g., $M = 5, 10, 15$ is selected for further investigation. Fig. 8 plots RUAVs energy consumption versus different number of USVs. One can observe the higher number of RUAVs leads to higher USVs energy consumption. Specifically, when $v = 2$ m/s and $I = 15$, USVs energy consumption is about 7.0×10^4 J when $M = 5$ while this value is nearly 1.0×10^5 J and 1.3×10^5 J when $M = 10$ and 15, respectively. Moreover, one can see that a higher number of USVs realizes a higher RUAVs energy consumption. In particular, when $M = 10$, RUAVs energy consumption is about 9.0×10^4 J when $I = 12$ while this value is approximately 1.1×10^5 J and 1.5×10^5 J when $I = 21$ and 30, respectively. This is because each RUAV is required to depart and fly back to RUAV base station at the beginning and at the end of each service period; even though the higher number of RUAVs can serve a higher number of USVs simultaneously, RUAVs suffer considerably additional energy consumption. One should note that the RUAV flight speed v and fight power p_{RUAV} should be jointly considered to decrease RUAVs flight energy consumption, which can be selected as future research direction.

V. Conclution

In this paper, a novel RIS-assisted cooperative UAV-USV MEC network architecture is proposed, where we cooperatively deploy RIS-mounted TUAV and RUAVs to serve USVs computation and communication cooperation. The RUAVs energy consumption minimization problem is formulated by jointly considering TUAV hovering altitude, RIS phase shift vector, RUAV service selection indicator and RUAVs turning points. To solve the formulated problem, a heuristic solution is proposed. First, we decouple the original problem into three subproblems. Moreover, we propose the ADMM algorithm, ESA algorithm and SCA-based algorithm, respectively to tackle the joint optimization of RIS phase shift vector and TUAV hovering altitude subproblem, RUAVs service selection indicators subproblem and RUAVs turning points subproblem. The results showed that the proposed solution can significantly decrease RUAVs energy consumption and increase energy efficiency compared with a list of selected benchmark algorithms. Also, the performance of the proposed solution under different typical ADMM penalty coefficients and the number of RIS reflecting elements are explored.

Note that when designing UAV-mounted RIS-assisted wireless communication networks, the number of RIS reflecting elements may have a considerable impact on UAVs propulsion and hovering power consumption, especially for on-board battery-empowered UAVs. However, the analysis of the RIS deployment scheme is still an open issue in this emerging research area [32]. Further research can be focused on optimizing the number of TUAV-mounted RIS elements since this is the critical step to realizing multiple-RIS-assisted cooperative UAV-USV MEC network, where fixed RISs coated on shore building surfaces and flexible RISs carried by TUAVs/RUAVs are cooperatively employed to serve resource-limited USVs.

References

[1] G. Shao, Y. Ma, R. Malekian, X. Yan and Z. Li, "A Novel Cooperative Platform Design for Coupled USV–UAV Systems," IEEE Transactions on Industrial Informatics, vol. 15, no. 9, pp. 4913-4922, 2019.

[2] Y. Liao, X. Chen, J. Liu, Y. Han, N. Xu and Z. Yuan, "Cooperative UAV-USV MEC Platform for Wireless Inland Waterway Communications," IEEE Transactions on Consumer Electronics, vol. 70, no. 1, pp. 3064-3076, 2024.

[3] A. Pogaku, D. Do, B. Lee and N. Nguyen, "UAV-Assisted RIS for Future Wireless Communications: A Survey on Optimization and Performance Analysis," IEEE Access, vol. 10, pp. 16320-16336, 2022.

[4] Y. Liao *et al.*, "Energy Minimization of Inland Waterway USVs for IRS-Assisted Hybrid UAV-Terrestrial MEC Network," IEEE Transactions on Vehicular Technology, vol. 73, no. 3, pp. 4121-4135, 2024.

[5] W. Xu and L. Gu, "UAV Relay Energy Consumption Minimization in an MEC-Assisted Marine Data Collection System," Journal of Marine Science and Engineering, vol. 11, no. 12, pp. 2333, 2023.

[6] Q. Ai, X. Qiao, Y. Liao and Q. Yu, "Joint Optimization of USVs Communication and Computation Resource in IRS-Aided Wireless Inland Ship MEC Networks," IEEE Transactions on Green Communications and Networking, vol. 6, no. 2, pp. 1023-1036, 2022.

[7] S. Gong *et al.*, "Toward Smart Wireless Communications via Intelligent Reflecting Surfaces: A Contemporary Survey," IEEE Communications Surveys & Tutorials, vol. 22, no. 4, pp. 2283-2314, 2020.

[8] D. Tyrovolas *et al.*,"Energy-Aware Design of UAV-Mounted RIS Networks for IoT Data Collection," IEEE Transactions on Communications, vol. 71, no. 2, pp. 1168-1178, 2023.

[9] X. Qin *et al.*, "Joint Optimization of Resource Allocation, Phase Shift, and UAV Trajectory for Energy-Efficient RIS-Assisted UAV-Enabled MEC Systems," IEEE Transactions on Green Communications and Networking, vol. 7, no. 4, pp. 1778-1792, 2023.

[10] H. Mei, K. Yang, J. Shen and Q. Liu, "Joint Trajectory-Task-Cache Optimization with Phase-Shift Design of RIS-Assisted UAV for MEC," IEEE Wireless Communications Letters, vol. 10, no. 7, pp. 1586-1590, 2021.

[11] Z. Zhai, X. Dai, B. Duo, X. Wang and X. Yuan, "Energy-Efficient UAV-Mounted RIS Assisted Mobile Edge Computing," IEEE Wireless Communications Letters, vol. 11, no. 12, pp. 2507-2511, 2022.

[12] L. Zhang, Y. Sun, Z. Chen and S. Roy, "Communications-Caching-Computing Resource Allocation for Bidirectional Data Computation in Mobile Edge Networks," IEEE Transactions on Communications, vol. 69, no. 3, pp. 1496-1509, 2021.

[13] T. Shafique, H. Tabassum and E. Hossain, "Optimization of Wireless Relaying with Flexible UAV-Borne Reflecting Surfaces," IEEE Transactions on Communications, vol. 69, no. 1, pp. 309-325, 2021.

[14] Y Liao, L Liu, Y Song and N Xu, "Joint Communication-Caching-Computing Resource Allocation for Bidirectional Data Computation in IRS-Assisted Hybrid UAV-Terrestrial Network," Chinese Journal of Electronics, vol. 33, no. 5, pp. 1-11, 2024.

[15] F. Yang, J. Wang, H. Zhang, M. Lin and J. Cheng, "Multi-IRS-Assisted mmWave MIMO Communication Using Twin-Timescale Channel State Information," IEEE Transactions on Communications, vol. 70, no. 9, pp. 6370-6384, 2022.

[16] X. Yuan, Y. Hu, J. Zhang and A. Schmeink, "Joint User Scheduling and UAV Trajectory Design on Completion Time Minimization for UAV-Aided Data Collection," IEEE Transactions on Wireless Communications, vol. 22, no. 6, pp. 3884-3898, 2023.

[17] T. Shafique, H. Tabassum and E. Hossain, "Optimization of Wireless Relaying with Flexible UAV-Borne Reflecting Surfaces," IEEE Transactions on Communications, vol. 69, no. 1, pp. 309-325, 2021.

[18] Y. Li, H. Zhang, K. Long and A. Nallanathan, "Exploring Sum Rate Maximization in UAV-Based Multi-IRS Networks: IRS Association, UAV Altitude, and Phase Shift Design," IEEE Transactions on Communications, vol. 70, no. 11, pp. 7764-7774, 2022.

[19] Y. Liao, Y. Song, L. Liu and Y. Han, "Joint Deployment and Task Scheduling in IRS-assisted Wireless Inland Ship MEC Network," in IEEE 97th Vehicular Technology Conference (VTC2023-Spring), Florence, Italy, pp. 1-6, 2023.

[20] R. Feng, Z. Li, Q. Wang and J. Huang, "An ADMM-Based Optimization Method for URLLC-Enabled UAV Relay System," IEEE Wireless Communications Letters, vol. 11, no. 6, pp. 1123-1127, 2022.

[21] Q. Zhang, L. Yan, Z. Feng, K. Zhang and Y. Zhang, "Joint Vehicle Association and Power Allocation for Energy Efficient Connected Automated Vehicles," in IEEE Global Communications Conference, Madrid, Spain, pp. 1-6, 2021.
[22] M. Grant and S. Boyd, "CVX: Matlab Software for Disciplined Convex Programming," version 2.1, 2014.
[23] K. Shen and W. Yu, "Fractional Programming for Communication Systems-Part I: Power Control and Beamforming," IEEE Transactions on Signal Processing, vol. 66, no. 10, pp. 2616-2630, 2018.
[24] J. Li, M. Zhou, Q. Sun, X. Dai and X. Yu, "Colored Traveling Salesman Problem," IEEE Transactions on Cybernetics, vol. 45, no. 11, pp. 2390-2401, 2015.
[25] N. Onizawa, K. Katsuki, D. Shin, W. J. Gross and T. Hanyu, "Fast-Converging Simulated Annealing for Ising Models Based on Integral Stochastic Computing," IEEE Transactions on Neural Networks and Learning Systems, vol. 34, no. 12, pp. 10999-11005, 2023.
[26] Z. Yang, S. Bi and Y. Zhang, "Online Trajectory and Resource Optimization for Stochastic UAV-Enabled MEC Systems," IEEE Transactions on Wireless Communications, vol. 21, no. 7, pp. 5629-5643, 2022.
[27] C. Xu *et al.*, "Energy Consumption and Time-Delay Optimization of Dependency-Aware Tasks Offloading for Industry 5.0 Applications," IEEE Transactions on Consumer Electronics, vol. 70, no. 1, pp. 1590-1600, 2024.
[28] Z. Meng, Y. Chen, M. Ding and D. López-Pérez, "A New Look at UAV Channel Modeling: A Long Tail of LoS Probability," in IEEE 30th Annual International Symposium on Personal, Indoor and Mobile Radio Communications (PIMRC), Istanbul, Turkey, pp. 1-6, 2019.
[29] M. Li, S. He and H. Li, "Minimizing Mission Completion Time of UAVs by Jointly Optimizing the Flight and Data Collection Trajectory in UAV-Enabled WSNs," IEEE Internet of Things Journal, vol. 9, no. 15, pp. 13498-13510, 2022.
[30] Q. Li *et al.*, "UAV Altitude, Relay Selection, and User Association Optimization for Cooperative Relay-Transmission in UAV-IRS-Based THz Networks," IEEE Transactions on Green Communications and Networking, vol. 8, no. 2, pp. 815-826, 2024.
[31] M. Asim, M. ELAffendi and A. A. A. El-Latif, "Multi-IRS and Multi-UAV-Assisted MEC System for 5G/6G Networks: Efficient Joint Trajectory Optimization and Passive Beamforming Framework," IEEE Transactions on Intelligent Transportation Systems, vol. 24, no. 4, pp. 4553-4564, 2023.
[32] B. Zhang, K. Yang, K. Wang and G. Zhang, "Performance Analysis of RIS-Assisted Wireless Communications with Energy Harvesting," IEEE Transactions on Vehicular Technology, vol. 72, no. 1, pp. 1325-1330, 2023.

Yangzhe Liao received his BS degree in Measurement and Control Technology from Northeastern University, China in 2013 and PhD degree from the University of Warwick, UK, in 2017. Currently, he is an associate professor at the School of Information Engineering, Wuhan University of Technology, China. His research interests include mobile edge computing and mobile computing.

Yuanyan Song obtained his BS degree from the Wuhan University of Technology, China in 2022. Currently, he is pursuing her master's degree at the School of Information Engineering, Wuhan University of Technology, China. His research interests including mobile edge computing and networking.

Siyu Xia obtained her BS degree from the South China University of Technology in 2014 and Master degree from the University of Warwick, UK in 2016. Currently, she is the librarian at the University Library, Wuhan University of Technology. Her research interests mainly focus on education informationization, big data and practical mathematical optimization.

Yi Han received the BEng. degree from the International School of Software, Wuhan University, China, in 2010, and the MS degree in telecommunication from Dublin City University, Ireland in 2011. He then obtained the PhD degree from the Performance Engineering Laboratory, University College Dublin, Ireland. He is currently an associate professor with the School of Information Engineering, Wuhan University of Technology, China. His research interests include QoE assessment and performance-aware adaptive multimedia delivery.

Ning Xu received his Ph.D. degree in Electronic Science and Technology from the University of Electronic Science and Technology of China, Chengdu, in 2003. Later, he was a postdoctoral fellow with Tsinghua University, Beijing, from 2003 to 2005. Currently, he is a professor at the School of Information Engineering of Wuhan University of Technology, Wuhan. Dr. Xu's research interests include computer aided design of VLSI circuits and systems, image processing, big data analysis, and artificial intelligence.

Xiaojun Zhai is currently a Reader in the Embedded Intelligent Systems Laboratory at the University of Essex. He has authored/co-authored over 140 scientific papers in international journals and conference proceedings. His research interests mainly include the design and implementation of the digital image and signal processing algorithms, custom computing using FPGAs, embedded systems, and hardware/software co-design.